



Cite this: *RSC Adv.*, 2020, 10, 44815

# Surface cross-linked thermoplastic starch with different UV wavelengths: mechanical, wettability, hygroscopic and degradation properties

Peng Yin,<sup>a</sup> Chunhao Chen,<sup>a</sup> Hongpeng Ma,<sup>a</sup> Huijuan Gan,<sup>a</sup> Bin Guo  <sup>\*abc</sup> and Panxin Li<sup>bc</sup>

Here, we report a method to improve the properties of thermoplastic starch (TPS) by surface ultraviolet (UV) cross-linking. TPS sheets were prepared by injection molding and coated with an ethanol solution of photo-initiator TPO (2,4,6-trimethyl benzoyl diphenyl phosphine oxide), then, irradiated by UV with different wavelengths for 15 min. Untreated and irradiated TPS sheets were characterized using tensile and bending tests, impact tests, dynamic mechanical thermal analysis (DMTA) and infrared spectroscopy (FTIR). FTIR spectra showed that UV irradiation can effectively trigger surface cross-linking of TPS sheets. The mechanical and dynamic mechanical properties of the TPS were improved and the optimized properties were obtained by 308 nm UV irradiation. A tensile strength of 4.1 MPa, a bending strength of 2.7 MPa, an impact strength of 96.8 kJ m<sup>-2</sup>, and the corresponding activation energy of 251.22 kJ mol<sup>-1</sup> were obtained. The water contact angle and moisture absorption of the samples were also investigated and the 308 nm UV irradiated sheets have a contact angle of 74°. Moisture absorption rate as a function of the square root of time showed a sigmoid curve including a linear stage which conforms to Fick's second law. The samples irradiated by 308 nm UV had the lowest equilibrium moisture absorption rate  $M_{\infty}$  and the longest time  $T_0$  to enter into the Fick's diffusion stage and the lowest slope  $K$  and diffusion coefficient  $D$ . All samples displayed biodegradable properties when buried in soil. This method has potential applications for agricultural mulch films, packing and medical film products.

Received 3rd September 2020  
Accepted 7th December 2020

DOI: 10.1039/d0ra07549c

rsc.li/rsc-advances

## 1. Introduction

Great attention has been paid to environmentally friendly biodegradable materials over the last two decades.<sup>1</sup> As a natural biopolymer, starch is abundant, renewable, biodegradable, and low cost, and is considered as one of the promising raw materials for developing biodegradable plastics especially in sustainable packaging.<sup>2</sup> Nowadays, thermoplastic starch (TPS) cannot be used widely because of retrogradation and unsatisfactory mechanical properties, particularly in wet and dry environments.<sup>3,4</sup> In order to improve the mechanical and water resistant properties of TPS, some strategies have been adopted: (1) adding reinforcing fillers in the starch matrix such as inorganic minerals,<sup>5</sup> and organic fibers;<sup>6,7</sup> (2) acetylation,<sup>8</sup> oxidation<sup>9</sup> of hydroxyl groups of the starch chains; (3) cross-linking modification of starch.<sup>10</sup>

Cross-linking modification is an efficient method in limiting excessive water swelling and macromolecular motion of the

starch matrix and thus avoid ageing. Treating granular starch with chemical cross-linking agent in heterogeneous media was made early in 1973 in which epichlorohydrin was used as cross-linker.<sup>11</sup> Other cross-linking agent such as sodium trimetaphosphate and phosphoryl chloride were also reported to improve the property of starch.<sup>12–14</sup> Although properties improvement has been made, use of chemical agents in starch modifications is still not recommended because of its increased processing costs and environmental and health issues.<sup>15</sup> As an alternative method, radiative treatment such as gamma irradiation, electron beam irradiation, and photo-irradiation depending on the ionising sources either in the solid state or liquid state has been widely considered,<sup>16,17</sup> and has been claimed to covalent cross-link of the polymer chain and improve the properties of the polymer.<sup>18</sup>

Unlike gamma irradiation or electron beam, UV light provides lower energy and cannot directly cleave the C–C or C–H bonds of starch molecules during the short periods of exposure time and is an energy-saving, environmental friendly and easy to operate modification method.<sup>19</sup> In literature, both bulk and surface cross-linking are taken. *e.g.*, Joly *et al.* present to use UV exposure to cross-link the thermoplastic starch after extruding the TPS film containing a low percentage of sensitizer, which is a bulk photo-crosslinking.<sup>20</sup> Unlike bulk photo-crosslinking,

<sup>a</sup>College of Science, Nanjing Forestry University, Nanjing 210037, China. E-mail: gbm@ustc.edu; Tel: +86 25 85427625

<sup>b</sup>Agricultural and Forest Products Processing Academician Workstation, Luohe 462600, China

<sup>c</sup>Post-Doctoral Research Center of Nanjiecun Group, Luohe 462600, China



modification on the surface of thermoplastic starch is an interesting approach which can change some surface properties of materials without using large amount of organic solvent and give rise to environmental and health concerns. Moreover, comparing with the bulk photo-crosslinking, the amounts of sensitizers used in surface photo-crosslinking was significantly lower, and the cross-linking reaction in the surface layer would be easier. Zhou *et al.* (2008) soaked the starch sheets in a photosensitizer sodium benzoate aqueous solution and cross-linked by UV irradiation.<sup>21</sup> The results of water contact angle measurements and moisture absorption measurements showed that surface photo-crosslinking modifications significantly reduced the hydrophilic character of the starch sheet surface and enhanced water resistance of the starch sheets. Niazi *et al.* (2015) use UV cross-linking as a tool to steer the mechanical properties of TPS based films. Sodium benzoate was used as photosensitizer in the process and the films' retro-gradation was suppressed at 50% and 100% relative humidity.<sup>22</sup>

TPO (2,4,6-trimethyl benzoyl diphenyl phosphine oxide) was found to have the highest efficiency to manipulate the photo cross-linking process in microcapsules.<sup>23</sup> So, TPO was used as photoinitiator in this study. TPS samples were prepared by injection molding and then coated with TPO/ethanol solution. Aiming to guarantee the efficiency of radical production of TPO and the following cross-linking of starch, three different UV wavelengths were chosen according to the UV absorption spectrum of TPO. We mainly focused on the effect of different UV wavelengths on mechanical (tensile, bending and impact), dynamic mechanical properties, surface wettability, hygroscopicity, and degradation properties of the TPS in this study.

## 2. Materials and methods

### 2.1 Materials

The corn starch (moisture content is 13.6 wt%, amylose content is 27%) was provided by Shandong Hengren Industry and Trade Company (Zaozhuang, China). Glycerin (CP) and ethanol were purchased from Sinopharm Holding Chemical Reagent Co., Ltd. (Shanghai, China). TPO was purchased from Nanjing Wali Chemical Technology Co., Ltd. (Nanjing, China). NaCl, NaBr, KCl, K<sub>2</sub>SO<sub>4</sub> were provided by Nanjing Jiaozi Teng Scientific Equipment Co., Ltd. (Nanjing, China).

### 2.2 Preparation of UV surface crosslinked TPS

The starch and glycerin were pre-mixed manually at a ratio of 3 : 1, and the mixture was fed to a twin-screw plastic extruder running at 150 rpm (SHJ20, Nanjing, China). TPS dumbbell-shaped samples were prepared by injection molding machines (BV90, Shanghai, China). The 2 wt% TPO was prepared by dissolving 2 g TPO in 100 mL absolute ethanol, and then uniformly coated on the surface of the sample with a brush. The sample surface was irradiated with a UV mini-crosslink machine (SCIENTZ03-II, Ningbo, China) at 254, 308 and 365 nm UV wavelength for 15 min, respectively. The process was illustrated in Fig. 1.

### 2.3 Mechanical measurements

After injection molding, the samples were immediately placed in some polyethylene bags to avoid moisture absorption and regeneration. Before testing, all samples were stored at a temperature of  $23 \pm 2$  °C and humidity of 50% according to the ASTM D638 test standard. The tensile and bending test was then performed on a testing machine (E44.304, MTS, Shenzhen, China) at room temperature in accordance with ASTM D638. Impact measurement was performed on a testing machine (501J, Wance, Shenzhen, China) under the ASTM D256-10. Five to eight replicates were carried out per formulation.

Dynamic mechanical thermal analysis (DMTA) was performed using a Netzsch 242E instrument (NETZSCH 242E, Germany) in a three-point bending mode at a frequency of 1, 3.3, 5, 10 Hz. The temperature is in the range of  $-120$  to  $120$  °C, and the heating rate is  $3$  °C min<sup>-1</sup>.

### 2.4 Spectral analysis

**2.4.1 Ultraviolet spectrum analysis.** UV absorption of TPO was measured at wavelength ranges of 200 nm to 400 nm, using a UV-2700 Ultraviolet-visible (UV-vis) spectrophotometer (Shimadzu, Japan).

**2.4.2 Fourier transforms infrared spectroscopy.** A Fourier transform infrared spectrometer (VERTEX 70, Bruker, Germany) was used to record the absorbance spectra of the TPS samples in attenuated total reflectance (ATR) mode. Powder samples were pressed by potassium bromide. IR spectra was measured at wavelengths from  $500$  cm<sup>-1</sup> to  $4000$  cm<sup>-1</sup>.

### 2.5 Contact angle

Measurement of the contact angle was carried out at room temperature. The wetting behavior of the samples was measured and analyzed using a contact angle analyzer (DSA100, KRÜSS, and Germany) and a watered syringe. A drop of water was dropped on the sample, and its angle of incidence was measured soon after deposition using software. Each photo was taken for 0.016 s to 1 s.

### 2.6 Moisture absorption process and model

The sample was cut into small pieces of about  $15 \times 15$  mm and equilibrated for 24 h at room temperature. Configure saturated NaBr solution (57% relative humidity at room temperature), saturated NaCl solution (75% relative humidity at room temperature), saturated KCl solution (84% relative humidity at room temperature), and saturated K<sub>2</sub>SO<sub>4</sub> solution (98% relative humidity at room temperature) in a desiccator and, then put the samples in it for moisture absorption test. At set intervals, the samples were taken out and weighed. The moisture absorption was calculated according to the following equation:

$M_t = \frac{W_t - W_0}{W_0} \times 100$ , where  $W_t$  is the weight of the sample at time  $t$  (g),  $W_0$  is the initial weight of the sample. When the weight of the sample changed little and almost no moisture was absorbed, that is, the moisture absorption reached equilibrium, the  $M_t - t^{1/2}$  curve was drawn. The slope  $K$  of the linear stage of



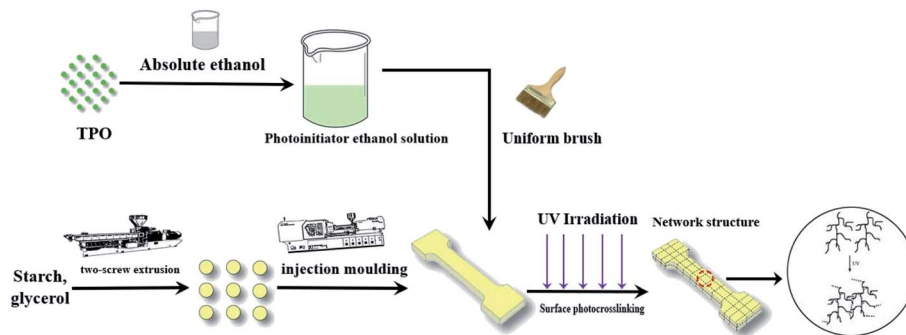


Fig. 1 Schematic of the preparation of UV cross-linked TPS samples.

moisture absorption curve can be obtained by the formula:  $K = \frac{M_{t_1} - M_{t_2}}{\sqrt{t_1} - \sqrt{t_2}}$ , in which  $M_{t_1}$  and  $M_{t_2}$  are the moisture absorption (%) of the sample at time  $t_1$  and  $t_2$ , respectively. In this stage, the diffusion behavior of water complies with the Fick's second law:  $\frac{\partial M}{\partial t} = D \frac{\partial^2 M}{\partial z^2}$ . In the formula:  $D$  is the diffusion coefficient;  $M$  is the amount of moisture absorption;  $t$  is the time of moisture absorption;  $z$  is the thickness direction of the sample. The diffusion coefficient  $D$  can be obtained by the separation variable method and expressed as follows:  $D = \pi \left( \frac{h}{4M_\infty} \right)^2 \left( \frac{M_{t_1} - M_{t_2}}{\sqrt{t_2} - \sqrt{t_1}} \right)^2$ , where  $h$  is the thickness of the sample.

## 2.7 Soil burial test

A soil burial test was carried out according to Riyajan *et al.*<sup>24</sup> The soil medium was poured into a plastic tray up to a thickness of approximately 18 cm. The samples were buried under 10 cm of soil, at an ambient temperature ( $\sim 25^\circ\text{C}$ ) with a humidity conditions of 70–80%. After that, water was sprayed twice a day to sustain the moisture in the medium. Every three days, the samples were collected and reweighed. The weight loss was calculated using equation as follows: weight loss (%) =  $[(W_0 - W_t)/W_0] \times 100$ , where  $W_0$  and  $W_t$  is the weight of the sample before and after the soil burial test, respectively.<sup>25</sup>

## 2.8 Statistical analysis

For mechanical property measurement, five to eight specimens of each formulation were tested as mentioned above. Other

measurements were repeated three times. Mean  $\pm$  SD of every measurements was reported in the manuscript. SD was calculated and given by Origin Pro 8 software.

## 3. Results and discussion

In order to improve the properties of TPS, surface photo cross-linking was taken in this study. TPS samples were prepared by injection molding and then coated with TPO solution. Different wavelengths were selected to irradiate TPS samples with the aim to efficiently trigger cross-linking between starch macromolecules. It is expected that UV irradiation will help to improve the mechanical and hydrophobic properties of TPS without affecting its degradation property.

### 3.1 Spectral analysis

UV absorption efficiency of photo initiator can affect the primary radical production and the following inter-molecules cross-linking of starch. So, the UV absorption spectrum of TPO in ethanol solution was determined and presented in Fig. 2a. It can be seen that the absorption peak of TPO is at 250, 296 and 380 nm, which is in accordance with the previous study.<sup>23</sup> In this study, three different wavelengths including 254, 308, and 365 nm which are close to the maximum absorption of TPO were selected to investigate the effect of UV wavelength on the properties of TPS. Under these UV irradiation, TPO was deduced to decompose to benzoyl and phosphoryl which is  $\alpha$ -cleavage in a Norrish-type I photo-reaction, then, the produced free-radical triggered cross-linking between starch macromolecules.<sup>26</sup>

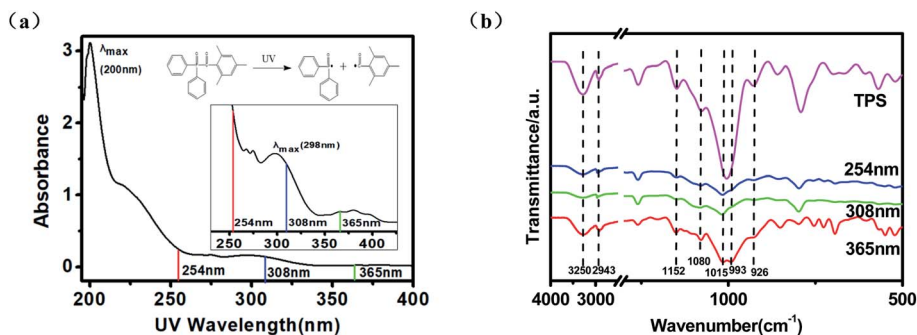


Fig. 2 (a) UV absorption spectrum of TPO; (b) ATR-FTIR spectra of untreated or irradiated TPS samples.



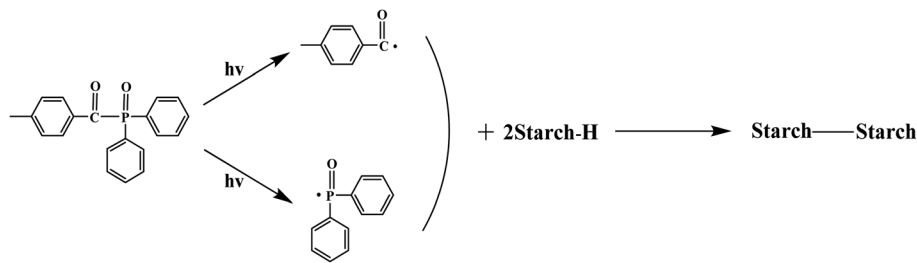


Fig. 3 Mechanism of TPO decomposition and cross-linking between starch macromolecules.

To see the possible chemical and physical interaction during photo cross-linking, ATR-FTIR spectroscopic analysis of the untreated and irradiated TPS samples was also carried out and the results were shown in Fig. 2b. The broad bands at  $3000\text{--}3500\text{ cm}^{-1}$  are ascribed to the stretching vibration of  $\text{--OH}$  of starch. This band became less intense when irradiated by UV, indicating the decrease of free  $\text{--OH}$  due to the cross-linking interaction between the starch chains.<sup>27</sup> Accordingly, the intense of the peaks at  $926$ ,  $1080$  and  $1152\text{ cm}^{-1}$  which are correspond to  $\text{C--O}$  stretching vibrations in  $\text{C--O--H}$  groups decreased. The intensity decrease of the bands at  $1006\text{ cm}^{-1}$  which can be assigned to the  $\text{C--O--C}$  bond stretching of the starch ring, especially after  $308\text{ nm}$  UV irradiation, also indicated the occurrence of cross-linking between starch chains.<sup>28,29</sup> The bands at  $993\text{ cm}^{-1}$ , which is related to intramolecular hydrogen bonding of the hydroxyl group at C-6 almost disappear when irradiated by  $308\text{ nm}$  UV wavelength. The mechanism of TPO decomposition and the following cross-linking of starch were shown in Fig. 3.<sup>19,30</sup>

### 3.2 Mechanical properties

The effect of both UV irradiation and their wavelength on the large strain behavior of TPS was analyzed up to their failure. The maximum tensile strength and elongation at break of TPS samples were shown in Fig. 4a. The tensile strength of TPS was obviously increased after irradiating by UV and have the maximum value of  $4.1\text{ MPa}$  for the TPS irradiated by  $308\text{ nm}$  UV, the TPS without irradiation is  $2.9\text{ MPa}$  and an increase of  $41.4\%$  was obtained. The elongation at break of the photo-irradiated TPS samples has no obvious decrease (from  $227.7$  to  $216\%$ )

compared with the untreated TPS. This mechanical improvement can be attributed to the cross-linking network structure formed on the surface of TPS by UV irradiation. Similar mechanical improvement was found in previous reports in which photo-crosslinked starch was prepared. *e.g.*, Niazi *et al.* (2015) prepared TPS films using surface photo-crosslinking and found that UV irradiation improved the mechanical properties and decreased the solubility and degree of swelling.<sup>22</sup> Kumar *et al.* (2008) investigated the effect of photo-crosslinking on the property of starch/cellulose composite films and found that both physical and mechanical properties were improved and the property increase was correlated with irradiation time.<sup>31</sup> Goudarzi *et al.* (2018) developed a photo-modified starch/kefir/TiO<sub>2</sub> bio-nanocomposite and found that increasing UV-A exposure time brought about an increase of  $14.9\%$  in the tensile strength of the bio-nanocomposites.<sup>32</sup>

In this study, TPS sheets were prepared instead of films, so, the bending and impact strength of TPS sheets was also determined (shown in Fig. 4b). All the irradiated samples have an increased bending and impact strength. The bending and impact strength of TPS irradiated by  $308\text{ nm}$  UV increased to  $2.7\text{ MPa}$  and  $96.8\text{ kJ m}^{-2}$ , which is obvious higher than TPS without UV irradiation ( $1.1\text{ MPa}$  and  $56.2\text{ kJ m}^{-2}$ ). Photo cross-linking efficiently improved the bending resistance and toughness of TPS materials.

### 3.3 Dynamic mechanical thermal properties

Fig. 5 is a three-dimensional mode of the storage modulus and loss factor curve in dynamic mechanical thermal analysis for untreated and UV irradiated TPS by performing a temperature

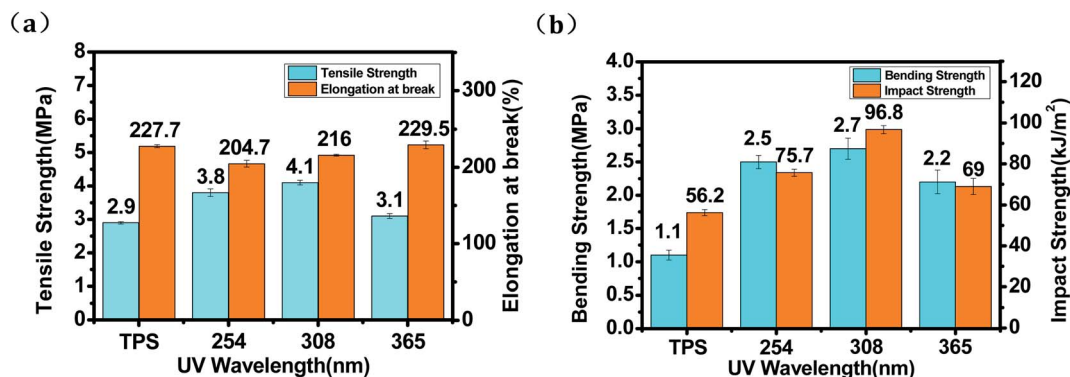


Fig. 4 Tensile strength, elongation at break (a) and bending, impact strength (b) of untreated TPS and irradiated TPS with different UV wavelengths.





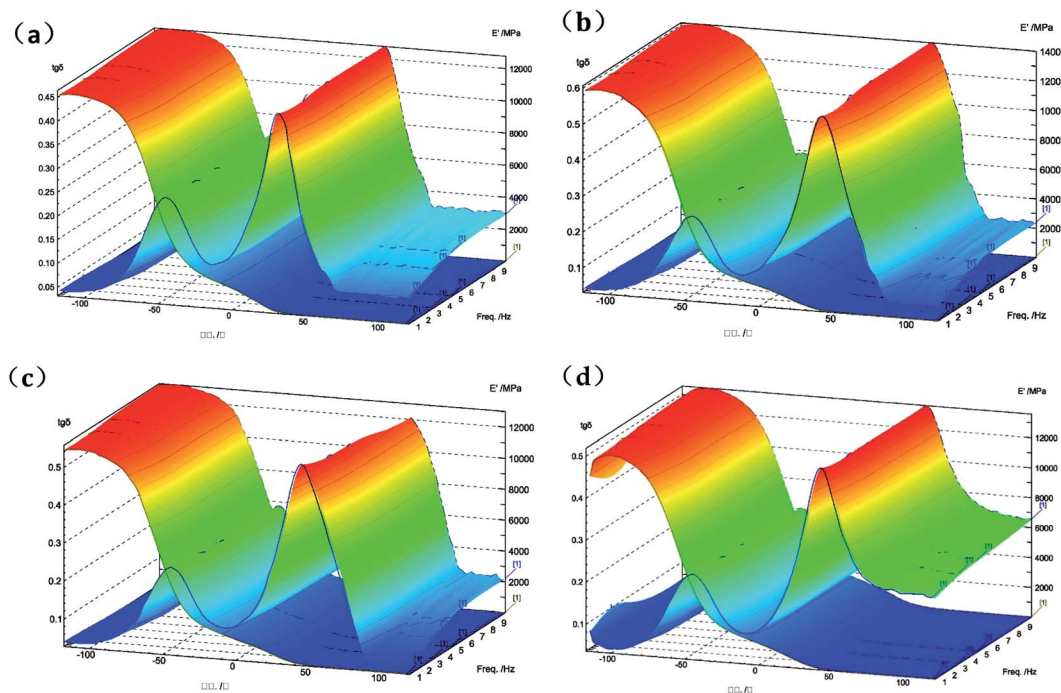


Fig. 5 3D DMA curves of untreated TPS (a) and TPS irradiated with UV wavelength of 254 nm (b), 308 nm (c), and 365 nm (d).

Table 1 Glass transition temperature and activation energy of untreated TPS and irradiated TPS with different ultraviolet wavelength

Sample	$T_{\beta}/^{\circ}\text{C}$ (5.000 Hz)	$T_{\alpha}/^{\circ}\text{C}$ (5.000 Hz)	$\Delta E_{\alpha}/(\text{kJ mol}^{-1})$
TPS	-40.57	35.34	205.99
254 nm	-40.51	47.27	246.60
308 nm	-37.48	50.32	251.22
365 nm	-39.46	45.17	243.96

scan at 1, 3.3, 5 and 10 Hz.  $T_g$  of the samples at 5.0 Hz from the loss factor curve was listed in Table 1.  $T_{\alpha}$  and  $T_{\beta}$  represents the  $T_g$  of the starch-enriched region and the glycerol-rich region in TPS, respectively.<sup>33,34</sup> Obviously,  $T_{\alpha}$  and  $T_{\beta}$  of TPS irradiated by UV are higher than that of the untreated TPS. The maximum value was observed in the TPS samples irradiated by 308 nm UV. This is also corresponded to the aforementioned mechanical analysis results. Formation of the cross-linked network structure on the surface of TPS samples restricted the movement of starch chains and thus led to higher transition temperature in the matrix.

The apparent activation energy,  $\Delta E$ , was calculated according to the relationship between the peak temperature,  $T_{\alpha}$  (K), and the frequency (Hz) of the tangent ( $\tan \delta$ ), using the following equation,<sup>35</sup>

$$\Delta E = 2.303R \frac{d \log f}{d(1/T)}$$

where  $T$  (K) is the peak temperature of the loss tangent,  $f$  (Hz) is the frequency, and  $R$  is the molar gas constant, which is  $8.3145 \text{ J mol}^{-1} \text{ K}^{-1}$ .  $\Delta E$  can be directly deduced from the slope of the graph of  $\log f$  with respect to  $1/T$ , and the results were also listed in Table 1. Apparently, the TPS irradiated by 308 nm UV has the highest activation energy, which provides another proof for the movement restriction of starch chains in the UV irradiated TPS samples.

### 3.4 Effect of ultraviolet wavelength on TPS surface contact angle

Surface water wettability of the samples was estimated by water contact angle analysis, shown in Table 2. It can be seen that surface cross-linking by UV irradiation significantly increased the

Table 2 Contact angle of untreated TPS and irradiated TPS with different UV wavelengths

Sample	TPS	254 nm	308 nm	365 nm
Angle ( $^{\circ}$ )	$34.28 \pm 1.9$	$70.64 \pm 1.4$	$75 \pm 3.2$	$56.8 \pm 0.8$
Images				



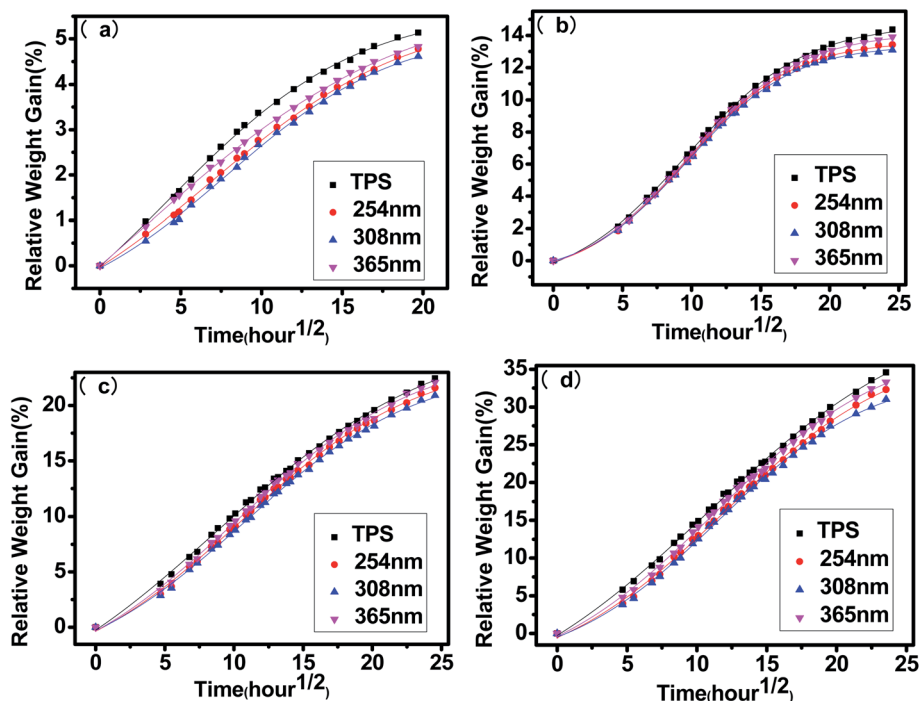


Fig. 6 Measured and fitted moisture absorption of untreated TPS and UV irradiated TPS by different UV wavelengths at (a) 57% humidity (b) 75% humidity (c) 84% humidity (d) 98% humidity.

surface contact angle. The maximum contact angle still exists in the samples irradiated by 308 nm UV and was  $75^\circ$ , as expected. The surface contact angle of the untreated TPS was  $34^\circ$ . These results indicated that surface cross-linking could decrease the wettability or enhance the hydrophobicity of the TPS sheets surface. The increment of water contact angle of the UV-irradiated sheets could be explained by the network structure formed on the surface of TPS samples which reduces the number of hydrophilic groups on the starch backbone, and this is also indicated by the results of ATR-FTIR analysis mentioned above.

### 3.5 Effect of ultraviolet irradiation on moisture absorption of TPS

Moisture absorption curves of untreated and irradiated TPS at different relative humidity of 57%, 75%, 84% and 98% were shown in Fig. 6. It can be seen that all samples showed similar variation trends of the relative weight gained as a function of time. There are two stages included in the process. At the first stage, the value of relative weight gained increased fast and reached a linear absorption as a function of the square root of time, then, the moisture absorption rate slows down and gradually approaches equilibrium state. As a whole, the moisture absorption rate of the irradiated samples is lower than the

Table 3 Hygroscopic kinetic parameters of untreated and irradiated TPS by different UV wavelengths

Relative humidity	Sample	$C_1$	$M_\infty$	$t_0$	$C_2$	$D$	$K$
57%	TPS	-4.2727	6.0051	2.7744	8.1584	0.01010	0.3406
	254 nm	-1.9091	5.5858	6.8416	6.2610	0.00767	0.2760
	308 nm	-1.2418	5.2170	7.8252	5.2754	0.00748	0.2547
	365 nm	-2.7601	5.6972	4.3063	5.88426	0.00895	0.3042
75%	TPS	-1.7215	14.7007	9.5903	4.2910	0.00687	0.6874
	254 nm	-1.1759	13.6529	9.6644	3.8337	0.00699	0.6440
	308 nm	-1.0712	13.4050	9.6768	3.8034	0.00708	0.6367
	365 nm	-1.3716	14.1950	9.7675	4.0496	0.00669	0.6550
84%	TPS	-9.3430	26.8056	8.8081	8.0803	0.00459	1.0244
	254 nm	-5.4452	24.4594	10.4316	6.5938	0.00452	0.9278
	308 nm	-4.8750	23.7291	10.6908	6.4481	0.00439	0.8871
	365 nm	-6.0677	25.1149	10.0840	6.7737	0.00461	0.9627
98%	TPS	-11.9571	43.9561	10.7428	8.0795	0.00384	1.5366
	254 nm	-6.5866	38.3669	11.8466	6.3510	0.00417	1.3986
	308 nm	-5.0267	34.9065	11.5166	5.6118	0.00483	1.3691
	365 nm	-7.1449	39.0313	11.2606	6.3808	0.00454	1.4840



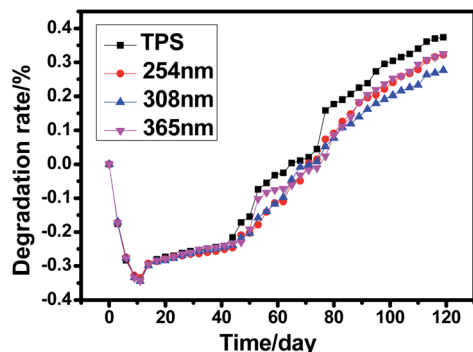


Fig. 7 Degradation curve of untreated and irradiated TPS during 120 days.

untreated one, and the TPS irradiated by 308 nm UV has the lowest moisture absorption rate. These results are in accordance with the aforementioned surface contact angle, which indicated that the UV irradiation increased surface water resistant ability and weakened the diffusion of water molecular which begins at the surface of the TPS materials.

To better understand the moisture absorption performance, sigmoidal fitting of the moisture absorption data in Fig. 6 is carried out, the fitted equation is expressed as follows:

$$M_t = \frac{C_1 - M_\infty}{1 + e^{(t-t_0)/C_2}} + M_\infty,$$

	Time/day	TPS	TPS-254nm	TPS-308nm	TPS-365nm
<b>a</b>	0				
	3				
	6				
	12				
	40				
	119				
<b>b</b>					

Fig. 8 Photos of the untreated and irradiated TPS sheets during the burial period (a) and the films formed in the irradiated TPS sheets (b).



where  $C_1$  and  $C_2$  are constants related to factors such as material and moisture absorption temperature;  $t$  is moisture absorption time;  $M_\infty$  is equilibrium moisture absorption rate;  $T_0$  is the start time of linear water absorption stage at which the diffusion of water conforms to Fick's second law. The key parameters during the water absorption of each sample are presented in Table 3 in which the symbol  $K$  represents the slope of the curve at the Fick's diffusion stage and  $D$  is the corresponding diffusion coefficient as mentioned in Section 2.6. As presented in the table, the equilibrium moisture absorption rate  $M_\infty$  of TPS decrease after UV irradiation whatever the relative humidity is. The TPS irradiated by 308 nm has the lowest value of  $M_\infty$ . Accordingly, the time  $T_0$  for the samples irradiated by 308 nm to enter into the Fick's diffusion stage is the longest, and the slope  $K$  and the diffusion coefficient  $D$  is the lowest. These results indicated that the photo cross-linking reaction at the surface of the samples provides a barrier function for moisture diffusion and this barrier property is most effective when irradiated by 308 nm UV. With the increasing of relative humidity, the diffusion coefficient  $D$  of each sample decreased and the slope  $K$  of the Fick's diffusion stage increased, accordingly, the equilibrium moisture absorption rate  $M_\infty$  increased. The plastication of water molecules improves the movement capacity of starch chain and thus facilitate the transfer of water in polymer materials.<sup>36,37</sup>

### 3.6 Effect of ultraviolet wavelength on TPS degradation property

The degradation rate of the samples was determined by the weight loss during burial time and the results were shown in Fig. 7. There are two main factors affecting the weight loss in this period: (1) the water absorption; (2) polymer degradation. The minus value of the degradation rate during the first 10 days was due to the higher water absorption than degradation, then, degradation rate increased gradually and reached maximum degradation rate after 40 days. Obviously, photo cross-linking lowered the degradation rate of TPS, and the TPS cross-linked by ultraviolet of 308 nm showed the lowest degradation rate. The starch degradation is due to the action of enzymes which is produced by fungi and/or bacteria in the soil, resulting in the formation of carbon dioxide, water and sugar.<sup>38</sup> Surface photo cross-linking formed a barrier against the microorganism's attack and thus decreased the degradation rate of TPS. Pictures of the samples during burial period (partial) were shown in Fig. 8. The samples mainly showed swelling property during the first 6 days. After that, samples were broken into pieces and became brown color after 40 days. Notably, a film was observed in the photo cross-linked TPS samples especially after a period of degradation (Fig. 8b) which further manifest that cross-linking occurred at the surface of TPS.

## 4. Conclusions

The thermoplastic starch can be effectively modified by UV cross-linking on its surface. The efficiency of cross-linking is related to the wavelength of UV which determines the efficiency of radical

production in photo initiator. For TPO, 308 nm UV has the highest trigger efficiency. The tensile, bending and impact strength of the TPS sheets coated with 2 wt% TPO/ethanol solution can be improved significantly by 308 nm UV irradiation for 15 min. Therefore, UV irradiation is a simple and efficient approach to improve the mechanical property of TPS. Meanwhile, surface photo cross-linking is also an efficient method to improve the water resistance and surface hydrophobic properties. The samples irradiated by 308 nm UV showed higher water contact angle, lower moisture absorption rate. All samples displayed biodegradation to some extent when buried in soil. The irradiated TPS materials are expected to be used in agricultural mulch film, packing and medical film in the future.

## Conflicts of interest

There are no conflicts to declare.

## Acknowledgements

The authors thank the Jiangsu Government Scholarship for overseas studies, Higher School in Jiangsu Province College Students' Practice Innovation Training Programs (201910298025Z), and the Natural Science Foundation of Jiangsu Province (BK20140967).

## References

- 1 M. A. Hillmyer, The promise of plastics from plants Plant-derived feedstocks are increasingly competitive in plastics production, *Science*, 2017, **358**, 868–870.
- 2 A. K. Mohanty, S. Vivekanandhan and J. M. Pin, Composites from renewable and sustainable resources: challenges and innovations, *Science*, 2018, **362**, 536–542.
- 3 M. B. K. Niazi, M. Zijlstra and A. A. Broekhuis, Influence of plasticizer with different functional groups on thermoplastic starch, *J. Appl. Polym. Sci.*, 2015, **132**, 42012.
- 4 A. L. M. Smits, P. H. Kruiskamp, J. J. G. van Soest and J. F. G. Vliegenthart, Interaction between dry starch and plasticisers glycerol or ethylene glycol, measured by differential scanning calorimetry and solid state NMR spectroscopy, *Carbohydr. Polym.*, 2003, **53**, 409–416.
- 5 R. Zhang, X. Wang and M. Cheng, Preparation and characterization of potato starch film with various size of nano-SiO<sub>2</sub>, *Polymers*, 2018, **10**, 1172.
- 6 B. Guo, L. J. Wang, P. Yin, B. G. Li and P. X. Li, Ultra-high molecular weight polyethylene fiber-reinforced thermoplastic corn starch composite, *J. Thermoplast. Compos. Mater.*, 2017, **30**, 564–577.
- 7 W. Zhou, D. D. Zha, X. Zhang, J. Xu, B. Guo and Y. N. Huang, Ordered long polyvinyl alcohol fiber-reinforced thermoplastic starch composite having comparable mechanical properties with polyethylene and polypropylene, *Carbohydr. Polym.*, 2020, **250**, 116913.
- 8 B. F. Bergel, S. D. Osorio, L. M. da Luz and R. M. C. Santana, Effects of hydrophobized starches on thermoplastic starch





- foams made from potato starch, *Carbohydr. Polym.*, 2018, **200**, 106–114.
- 9 Y. R. Zhang, X. L. Wang and G. M. Zhao, Influence of oxidized starch on the properties of thermoplastic starch, *Carbohydr. Polym.*, 2013, **96**, 358–364.
  - 10 L. P. Qiu, F. Hu and Y. L. Peng, Structural and mechanical characteristics of film using modified corn starch by the same two chemical processes used in different sequences, *Carbohydr. Polym.*, 2013, **91**, 590–596.
  - 11 L. Kuniak and R. H. Marchessault, Study of the crosslinking reaction between epichlorohydrin and starch, *Starch/Staerke*, 1973, **24**, 110–116.
  - 12 J. Jane, A. Xu, M. Radosavljevic and P. A. Seib, Location of amylose in normal starch granules. I. Susceptibility of amylose and amylopectin to cross-linking reagents, *Cereal Chem.*, 1992, **69**, 405–409.
  - 13 C. Yook, U. A. Pek and K. H. Park, Gelatinization and retrogradation characteristics of hydroxypropylated and cross-linked rices, *J. Food Sci.*, 1993, **58**, 405–407.
  - 14 K. Woo and P. A. Seib, Cross-linking of wheat starch and hydroxypropylated wheat starch in alkaline slurry with sodium trimetaphosphate, *Carbohydr. Polym.*, 1997, **33**, 263–271.
  - 15 J. Zhou, J. Zhang, Y. Ma and J. Tong, Surface photo-crosslinking of corn starch sheets, *Carbohydr. Polym.*, 2008, **74**, 405–410.
  - 16 N. Detduangchan and T. Wittaya, Effect of UV-treatment on properties of biodegradable film from rice starch, *World Acad. Sci. Eng. Technol.*, 2011, **5**, 829–834.
  - 17 J. Delville, C. Joly, P. Dole and C. Bliard, Solid state photocrosslinked starch based films: a new family of homogeneous modified starches, *Carbohydr. Polym.*, 2002, **49**, 71–81.
  - 18 M. B. K. Niazi and A. A. Broekhuis, Surface photo-crosslinking of plasticized thermoplastic starch films, *Eur. Polym. J.*, 2015, **64**, 229–243.
  - 19 G. J. He, Q. Liu and M. R. Thompson, Characterization of structure and properties of thermoplastic potato starch film surface cross-linked by UV irradiation, *Starch/Staerke*, 2013, **65**, 304–311.
  - 20 J. Delville, C. Joly and P. Dole, Solid state photocrosslinked starch based films: a new family of homogeneous modified starches, *Carbohydr. Polym.*, 2002, **49**, 71–81.
  - 21 J. Zhou, J. Zhang and Y. H. Ma, Surface photo-crosslinking of corn starch sheets, *Carbohydr. Polym.*, 2008, **74**, 405–410.
  - 22 M. B. K. Niazi and A. A. Broekhuis, Surface photo-crosslinking of plasticized thermoplastic starch films, *Eur. Polym. J.*, 2015, **64**, 229–243.
  - 23 X. W. Li, W. D. Lai, S. S. Meng and H. Y. Yu, Photoinitiator Influence on the Photo-crosslink Property in Polyurea Microcapsules, *J. Photopolym. Sci. Technol.*, 2009, **22**, 603–608.
  - 24 S. A. Riyajan, Y. Sasithornsonti and P. Phinyocheep, Green natural rubber-g-modified starch for controlling urea release, *Carbohydr. Polym.*, 2012, **89**, 251–258.
  - 25 M. Bootklad and K. Kaewtatip, Biodegradation of thermoplastic starch/eggshell powder composites, *Carbohydr. Polym.*, 2013, **97**, 315–320.
  - 26 K. Ruhland, F. Habibollahi and R. Horny, Quantification and elucidation of the UV-light triggered initiation kinetics of TPO and BAPO in liquid acrylate monomer, *J. Appl. Polym. Sci.*, 2020, **48357**, 1–16.
  - 27 H. J. Wu, Y. L. Lei, J. Y. Lu, R. Zhu, D. Xiao, C. Jiao, R. Xia, Z. Q. Zhang, G. H. Shen, Y. T. Liu, S. S. Li and M. L. Li, Effect of citric acid induced crosslinking on the structure and properties of potato starch/chitosan composite films, *Carbohydr. Polym.*, 2019, **97**, 105208.
  - 28 N. Gurler, S. Pasa, M. H. Alma and H. Temel, The fabrication of bilayer polylactic acid films from cross-linked starch as eco-friendly biodegradable materials: synthesis, characterization, mechanical and physical properties, *Eur. Polym. J.*, 2020, **127**, 109588.
  - 29 J. Brugnerotto, J. Lizardi, F. M. Goycoolea, W. Arguelles-Monal, J. Desbrieres and M. Rinaudo, An infrared investigation in relation with chitin and chitosan characterization, *Polymer*, 2001, **42**, 3569–3580.
  - 30 A. H. M. Zain, M. K. A. Wahab and H. Ismail, Solid-state photo-cross-linking of cassava starch: improvement properties of thermoplastic starch, *Polym. Bull.*, 2018, **75**, 3341–3356.
  - 31 A. P. Kumar and R. P. Singh, Biocomposites of cellulose reinforced starch: improvement of properties by photo-induced crosslinking, *Bioresour. Technol.*, 2008, **99**, 8803–8809.
  - 32 V. Goudarzi and I. Shahabi-Ghahfarrokhi, Development of photo-modified starch/kefir/TiO<sub>2</sub> bio-nanocomposite as an environmentally-friendly food packaging material, *Int. J. Biol. Macromol.*, 2018, **116**, 1082–1088.
  - 33 A. L. Da Roz, A. J. F. Carvalho, A. Gandini and A. A. S. Curvelo, The effect of plasticizers on thermoplastic starch compositions obtained by melt processing, *Carbohydr. Polym.*, 2006, **63**, 417–424.
  - 34 K. M. Dang and R. Yoksan, Development of thermoplastic starch blown film by incorporating plasticized chitosan, *Carbohydr. Polym.*, 2015, **115**, 575–581.
  - 35 N. Anousheh, F. O. Godey and A. Soldara, Unveiling the Impact of Regioisomerism Defects in the Glass Transition Temperature of PVDF by the Mean of the Activation Energy, *J. Polym. Sci., Part A: Polym. Chem.*, 2017, **55**, 419–426.
  - 36 L. R. Bao, A. F. Yee and C. Y. C. Lee, Moisture absorption and hygrothermal aging in a bismaleimide resin, *Polymer*, 2001, **42**, 7327–7333.
  - 37 L. R. Bao and A. F. Yee, Moisture absorption and hygrothermal aging in bismaleimide matrix carbon fiber composites-part I: uni-weave composites, *Compos. Sci. Technol.*, 2002, **62**, 2099–2110.
  - 38 S. M. M. Franchetti and J. C. Marconato, Polímeros biodegradáveis-uma solução parcial para diminuir a quantidade dos resíduos plásticos, *Quim. Nova*, 2006, **29**, 811–816.

